16th World Conference on Earthquake Engineering, 16WCEE 2017
Santiago Chile, January 9th to 13th 2017
Paper N° 4134
Registration Code: S-A1464717034

NONLINEAR FINITE ELEMENT MODELING OF REINFORCED CONCRETE STRUCTURAL WALLS

M. F. Gullu[(1)], K. Orakcal[(2)]

[(1)] Research Assist., Bogazici University, fethi.gullu@boun.edu.tr
[(2)] Assoc. Prof., Bogazici University, kutay.orakcal@boun.edu.tr

Abstract

A relatively simple finite element modeling methodology was developed for simulating the cyclic lateral load behavior of reinforced concrete structural walls with varying levels of coupling between nonlinear flexural and shear response components. The behavioral characteristics of the constitutive panel elements incorporated in the model formulation are based on a fixed-crack-angle modeling methodology, which is effectively a smeared-stress-strain-based strut-and-tie approach that does not require ad-hoc model parameters. The constitutive panel model formulation also incorporates simple yet effective behavioral models for the shear-aggregate-interlock effects in concrete and dowel action on reinforcing bars, constituting the shear stress transfer mechanisms across the cracks. The model formulation was implemented into Matlab and model response predictions were compared with experimentally-measured responses of selected wall specimens with varying geometry and reinforcement characteristics; including relatively slender (aspect ratio of 3.0) walls with rectangular and T-shaped cross-sections, squat walls (aspect ratio of 0.5) with shear-controlled responses, and medium-rise walls (aspect ratios of 1.5–2.0) with predominant shear-flexure interaction responses. The proposed finite element modeling approach demonstrates a reasonable level accuracy in predicting the nonlinear hysteretic response of the wall specimens investigated. Accurate predictions are obtained for the experimentally-measured response attributes of the walls; including their lateral strength, stiffness, and ductility, as well as their hysteretic response characteristics. The model also provides accurate estimates of the relative contribution of nonlinear flexural and shear deformations to wall lateral displacements, and local response characteristics (e.g., strain distributions). Based on the response comparisons presented, model capabilities are assessed and possible model improvements are identified. Overall, the modeling approach proposed, despite its relatively simple formulation, is shown to provide reliable predictions of the nonlinear lateral load behavior of reinforced concrete walls with various aspect ratios and response characteristics.

Keywords: Reinforced concrete; Wall; Model; Shear; Flexure

1. Introduction

Improving the seismic performance of reinforced concrete (RC) building-type structures with means to improve their lateral stiffness and lateral load capacity, promotes the use of structural walls. Structural walls are designed and detailed to provide adequate stiffness and strength, as well as sufficient ductility to attain favorable structural performance under moderate and severe earthquake demands. Codes and recommendations for design of new buildings enforce the walls to exhibit ductile flexural behavior, with sufficient shear capacity to prevent brittle failures. However, obtaining reliable predictions for local responses (e.g., compressive strain at boundary zones) and prediction of nonlinear shear behavior are still topics of interest for even slender structural walls. Robust characterization and analytical representation of the behavior of slender walls with different cross-sectional geometries, as well as medium-rise and squat structural walls under earthquake actions, is a significant area of research, towards a more reliable design and performance assessment RC buildings.

The aspect (height-to-width) ratio (h_w/l_w) is commonly used to classify structural walls. Shear behavior governs the response of structural walls with aspect ratios less than 1.0-1.5 (squat structural walls), whereas for structural walls with aspect ratios exceeding 2.5-3.0 (slender structural walls), flexural actions predominantly control the wall response. For structural walls with moderate aspect ratios (between 1.5 and 2.5), both flexural

yielding and nonlinear shear deformations (which are usually coupled) contribute to wall behavior. For such walls, nonlinear shear deformations can constitute up to 30% to 50% of lateral wall displacements, as investigated experimentally by Tran and Wallace [1]. Reliable behavioral modeling of such structural walls with predominant shear-flexure interaction (SFI) behavior is of particular interest, especially because fiber-based modeling methodologies commonly used in practice for performance-based design of buildings typically consider uncoupled shear and flexural response components. However, analytical models with uncoupled axial, flexure, and shear responses are shown by previous research to underestimate compressive strains even in relatively slender RC walls controlled by flexure [2], and overestimate the lateral load capacity of RC walls with moderate aspect ratios [1] and low aspect ratios [3]. So, there is a need for relatively simple modeling approaches that consider interaction (coupling) between axial, flexural, and shear responses, and capture important hysteretic response features for a wide range of wall geometries and reinforcing details.

Accordingly, in this study, the finite element modeling methodology developed by Gullu [4] was implemented and improved for simulating the lateral load behavior of RC structural walls under reversed cyclic loading conditions. The behavior of the constitutive panel elements in the finite element model formulation is described by a previously-developed constitutive relationship named as the Fixed-Strut-Angle Model [5, 6]. Improved constitutive models for shear aggregate interlock and dowel action mechanisms were implemented in the constitutive model formulation for simulating the transfer of shear stress across cracks. The finite element wall model with the improved constitutive formulation was calibrated for wall specimens with varying aspect ratios and geometries, where coupled flexural yielding and nonlinear shear deformations were observed, resulting in reduced lateral stiffness, strength and ductility. The model was calibrated for the relatively slender wall specimens tested by Thomsen and Wallace [7], medium rise wall specimens tested by Tran and Wallace [1] and the squat wall specimens tested by Massone [8], Orakcal et al. [9], and Terzioglu [10], and model predictions were compared with the experimentally-observed hysteretic lateral load vs. displacement responses.

2. Analytical Model Description

Finite element modeling of RC structural walls involves assembling of constitutive panel elements for obtaining the overall model of a wall. To represent the behavior of the wall model, the combination of hysteretic nonlinear material relationships along crack directions of the constitutive panel, together with behavioral response characteristics including compression softening, tension stiffening, hysteretic biaxial damage, and shear stress transfer across cracks are used in combination. The so-called Fixed Strut Angle Model (FSAM) originally proposed by Ulugtekin [5] was selected as the constitutive panel model in the finite element model assembly. Its simple formulation and adequate accuracy makes it a feasible candidate for implementation. The original FSAM model incorporates perfect bond assumption between concrete and reinforcing steel bars, which is reasonable under favorable anchorage conditions. The base assumption in the original FSAM is that crack directions coincide with principal stress directions in concrete, implying zero shear stress developing along the crack surface. After cracking, principal stress directions in concrete are fixed along the fixed strut (crack) directions, whereas principal strain directions are free to rotate. It neglects shear aggregate interlock effects in concrete along crack surfaces, and dowel action on reinforcing bars. However, the formulation of the FSAM was improved to incorporate shear aggregate interlock and dowel action effects for transfer of shear stresses across cracks. The behavior of concrete along the fixed compression struts within each panel element is represented using biaxial stress–strain relationships, whereas the behavior of reinforcing steel is described by uniaxial stress-strain relationships applied along the directions of reinforcing steel bars. The hysteretic stress–strain relationship for concrete by Chang and Mander [11] is adopted in the model formulation (Fig.1(a)), also considering biaxial compression softening and biaxial hysteretic damage effects. The reinforcing steel stress–strain relationship proposed by Menegetto and Pinto [12] is used to represent uniaxial hysteretic behavior of reinforcing bars (Fig.1(b)).

Prior to formation of the first crack in the FSAM, the stress–strain behavior of concrete is assumed to follow the monotonic envelope. It is assumed that the principal stress and strain directions coincide, and the stress–strain model for concrete is applied in the principal strain direction in a rotating manner (Fig.2(a)). When the principal tensile strain first exceeds the monotonic cracking strain of concrete, the first crack forms in the

FSAM, in perpendicular direction to the principal tensile strain. Thereby the first fixed strut develops, which is parallel to the direction of the first crack. The direction of the first strut (crack) remains constant during later loading stages, where the principal strain directions continue to rotate, whereas the principal stress directions, along which the concrete stress–strain relationship is applied, are fixed (Fig.2(b)).

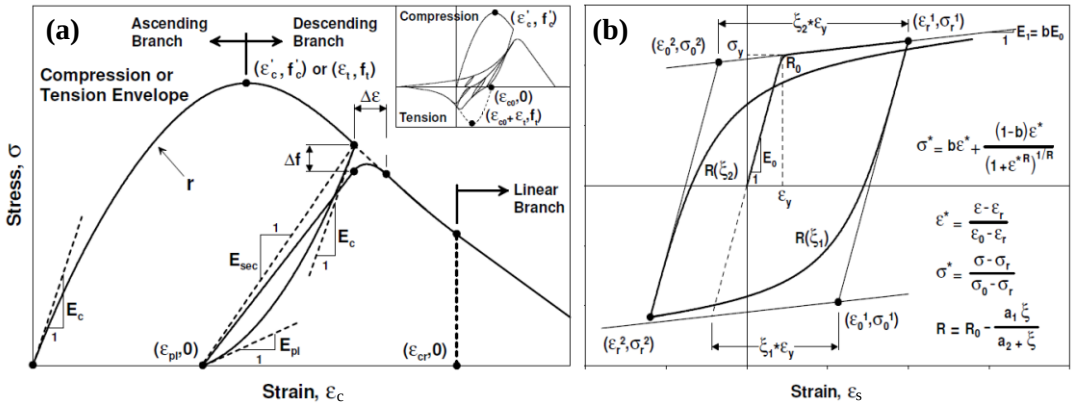

Fig. 1 – Material constitutive models: (a) Concrete [11], (b) Reinforcing steel [12]

As principal concrete stress and crack directions are assumed to coincide, no shear stress develops along the crack directions, implying zero aggregate interlock and zero dowel action assumptions in the base (original) formulation of the FSAM. This also implies that the second crack has to develop in perpendicular direction to the first crack. Before formation of the second crack, the stress–strain relationship is applied in parallel and perpendicular directions to the first crack, in the form of a single strut mechanism. When the tensile strain along the first strut exceeds the cracking strain of concrete, the second crack (and strut) develops perpendicular to the first crack direction. The biaxial behavior of concrete after formation of the second crack is shown in Fig.2(c). During further stages of loading, these two struts are subjected to tension or compression, and the concrete stress–strain model is applied along the two fixed strut (fixed principal stress) directions. The stress in the reinforcing steel bars is calculated using the uniaxial stress–strain relationship along the bar directions. The stresses developing in concrete and reinforcing steel bars are then superimposed (considering the reinforcement ratios) to obtain the average (smeared) stresses developing in the reinforced concrete panel element.

The original formulation of the FSAM, in which the aggregate interlock and the dowel action mechanisms are ignored, was later modified since the assumption that no shear stress transfer occurs across crack surface may lead to overestimation of shear deformations and prediction of premature sliding shear failures. To remedy this shortcoming of the original FSAM, Orakçal et al. [6] proposed a simple friction-based elasto-plastic aggregate interlock model, generating sliding shear stresses on crack surfaces (Fig.3(a), (b)). In this interlock model, when the normal stress perpendicular to the crack surface is tensile, the sliding stress effect is assumed to be zero. When the normal stress perpendicular to the crack surface is compressive, the sliding shear stress is bounded by the product of that compressive stress and a shear friction coefficient (e.g., $\mathbf{h}$=1.0).). In addition, while sliding shear stresses on the crack surface resulting from the compressive stress in concrete follows elasto-plastic hysteretic behavior (Fig.3(b)), those resulting from the clamping force of the reinforcing steel bars are assumed to follow an origin-oriented hysteretic behavior (Fig.3(c)), with the capacity calculated based on the shear-friction approach in ACI-318-11. In this study, contribution of the compressive stress in concrete perpendicular the crack surface was considered using a friction coefficient $\mathbf{h}$ = 1 for all type of structural walls, based on sensitivity studies conducted using the model on previously-conducted tests on squat RC walls experiencing sliding shear failure [9]. Contribution of the clamping force created by the reinforcing steel bars to the shear friction capacity was represented using a friction coefficient of approximately $\mathbf{h}_{st}$ = 0.5 for the wall specimens. Also, cyclic strength degradation parameters were implemented in the constitutive models for contribution of the clamping effect on aggregate interlock and the dowel action, using the equations proposed by Thermou *et al.* [13], as described by Karabulut [14]. In the present study, the elasto-plastic dowel action model proposed by He and Kwan [15] was implemented as the monotonic envelope of the dowel force vs. shear strain constitutive

relationship, and the origin-oriented unloading and reloading paths previously adopted by Horoz et al. [16] were used to for modeling of the wall specimens investigated (Fig.3(d)).

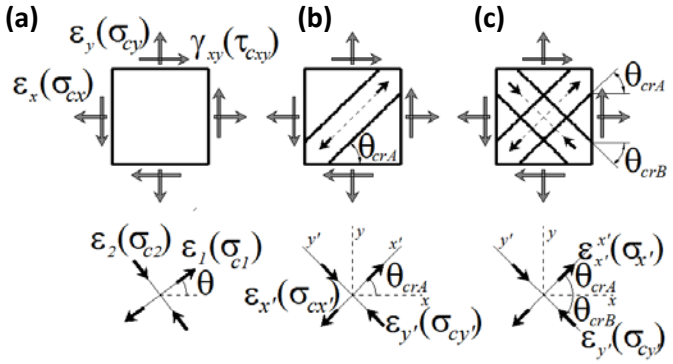

Fig. 2 – Fixed Strut Angle Model (FSAM) – concrete behavior a) Uncracked behavior, b) Behavior after formation of first crack, c) Behavior after formation of second crack [17]

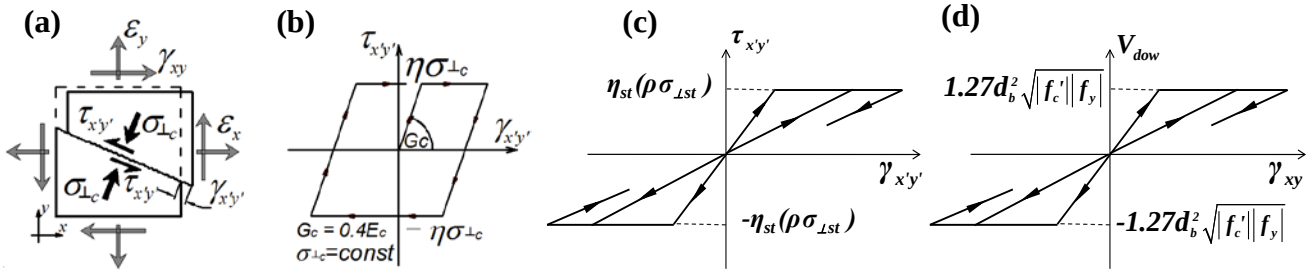

Fig. 3 – a) Strains and stresses along a crack [6], b) Friction-based constitutive model for contribution of concrete stress to aggregate interlock [6], c) Contribution of clamping on reinforcing bars on aggregate interlock, d) Dowel action model [16]

3. Comparison of Analytical Results with Test Results

For experimental validation of the model, experimental results obtained for three of the five medium-rise wall specimens tested by Tran and Wallace [1] were first used. These specimens were characterized by their aspect ratios (1.5 and 2.0), axial load levels ($0.025A_g f_c'$ and $0.10A_g f_c'$), and reinforcement configurations at boundary and web regions. The geometry and reinforcement details for the three wall specimens used for validation of the model are shown in Fig.4(a), Fig.4(b) and Fig.4(c). Concrete with compressive strength of 34.5 MPa and boundary reinforcement with yield strength of 414 MPa were used in the construction of these specimens. The analytical model was also validated using the experimental results for relatively slender (h_w/l_w = 3) wall specimens having rectangular and T-shaped cross-sections, provided by Thomsen and Wallace [7] (Fig.4(e), Fig.4(f)). Two of the eleven squat wall specimens having different aspect ratios and different reinforcement configurations tested by Terzioğlu [10] were also used to validate the analytical model. These two squat wall specimens (h_w/l_w = 0.5) were differentiated from each other by the axial load level. The dimensions and reinforcement details of the specimens are provided in Fig.4(g) and Fig.4(h). The concrete compressive strength varied between 19 and 35 MPa for these specimens, whereas the reinforcing bar yield strength varied between 440 MPa and 575 MPa. Two wall pier specimens having a shear span-to-depth ratio of 0.44 tested by Massone [8] and Orakcal et al. [9] were used for further validation of the model. Fig.4(d) shows the dimensions and the reinforcement details of the two identical specimens with different concrete compressive strength values and constant axial load levels. The concrete compressive strength of these specimens varied between 28.3 and 32.0 MPa, whereas the rebar yield strength was 424 MPa.

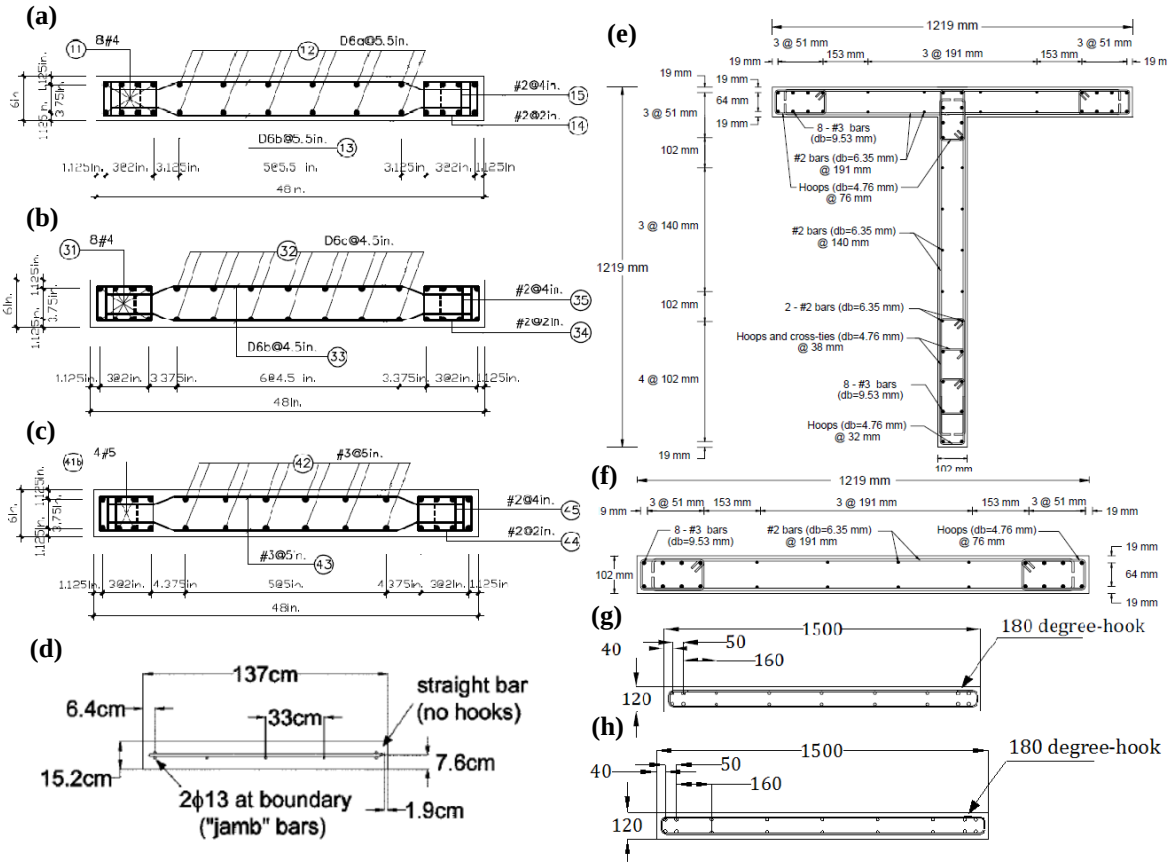

Fig. 4 – Wall cross-sectional views: a) RW-A20-P10-S38 [1], b) RW-A15-P10-S51 [1], c) RW-A15-P10-S78 [1], d) WP-T5-N5-S1 and WP-T5-N5-S2 [8,9], e) TW2 [7], f) RW2 [7], g) SW-T1-S1-2 [10], h) SW-T1-N10-S1-11 [10]

Properties of the wall specimens used to verify the analytical models are summarized in Table 1. The first three sets of specimens incorporated a RC pedestal at the bottom for connection of the specimen to the laboratory strong floor, and a RC or steel load transfer beam at the top for connection of the specimen to the loading actuator. Lateral loading on the specimens was applied by an actuator, one end which it fixed to a reaction wall. All walls were tested under reversed cyclic lateral loads, while the axial loads on the specimens were kept constant. The two squat wall specimens tested by Massone [8] and Orakcal et al. [9] had a different test setup from the other specimens. They tested under zero rotation at both ends (beam and pedestal), a constant axial load, and cyclic lateral load applied at mid-height level of the specimens, creating a double-curvature loading condition where the bending moment on each wall is zero at wall mid height and maximum (with reverse signs) at the top and bottom cross-sections of the wall, representing the actual loading conditions on wall piers and spandrels in a perforated perimeter wall of a building.

The finite element model configurations used for modeling and analysis of the test specimens were calibrated for several aspects of the wall specimens, including the geometric properties, reinforcement attributes, material characteristics, and loading conditions. As-tested properties of the materials employed in the construction of the specimens are used to calibrate the constitutive material parameters used in the model formulation. In calibration of the parameters for concrete and reinforcing steel in tension, tension stiffening effects were also considered. As well, the constitutive material parameters were also calibrated in terms of the existing compressive and the tensile stress-strain curves of concrete. Model predictions were compared with test results both at global (lateral load–displacement) and local (deformations) response levels for all specimens. The local response comparisons presented in this paper include flexural and shear deformation contributions to lateral displacement and longitudinal strain profiles for selected specimens.

Table 1 – Geometry and reinforcement details for wall specimens

	Specimen		Height (cm)	Length (cm)	Aspect Ratio	$P_{ax}/A_g f_c'$	Web Reinf. (Transverse / Longitudinal)		Boundary Reinforcement	
							Reinforcing Bar	ρ (%)	Reinforcing Bar	ρ_b (%)
Tran and Wallace (2012)	RW-A20-P10-S38		244	122	2.00	0.10	6.00 mm @ 140 mm	0.27	8 x 12.70 mm	3.23
	RW-A20-P10-S51		183	122	1.50	0.10	6.00 mm @ 114 mm	0.32	8 x 12.70 mm	3.23
	RW-A15-P10-S78		183	122	1.50	0.10	9.53 mm @ 127 mm	0.73	4 x 19.05 mm 4 x 15.87 mm	6.06
Thomsen and Wallace (1995, 2003)	RW2		366	122	3.00	0.07	6.35 mm @ 191 mm	0.33	8 x 9.53 mm	2.93
	TW2	Web	366	122	3.00	0.08	6.35 mm @ 140 mm	0.44	8 x 9.53 mm	2.93
		Flange					6.35 mm @ 191 mm	0.33	8 x 9.53 mm	2.93
Terzioğlu (2011)	SW-T1-S1-2		75	150	0.50	0.00	ϕ8 @ 250 mm	0.34	4 ϕ 16	5.15
	SW-T1-N10-S1-11		75	150	0.50	0.10	ϕ8 @ 250 mm	0.34	4 ϕ 16	5.15
Wallace et al. (2006)	WP-T5-N5-S1		137	122	0.44	0.05	ϕ13 @ 305 / 330 mm	0.278 / 0.227	2 ϕ 13	1.33
	WP-T5-N10-S2		137	122	0.44	0.10	ϕ13 @ 305 / 330 mm	0.278 / 0.227	2 ϕ 13	1.33

In Fig.5, analytical model results were compared with the global and local-level experimental responses for the medium rise wall specimens investigated. For specimens RW-A20-P10-S38 and RW-A15-P10-S51, lateral strength degradation (failure) initiated with crushing of core concrete in wall boundaries and buckling of longitudinal boundary reinforcement. Strength degradation due to widening of the diagonal cracks was also observed during the tests. As shown in Fig.5(a) and Fig.5(b), the analytical model results are in agreement with the test results for these two specimens, in terms of lateral load capacity and ductility, as well as other important response characteristics such as stiffness degradation, plastic deformations and pinching. For specimen RW-A15-P10-S78, which experienced failure due to crushing of the diagonal compression strut at wall base, model predictions presented in Fig.5(c) are again reasonable. Analytical model predictions were compared with test results at also local (deformation) response levels. It is shown in Fig.5(d) and Fig.5(e) that the model can successfully simulate the highly-pinched lateral load vs. shear deformation response and the ductile lateral load vs. flexural deformation response characteristics of specimen RW-A15-P10-S78. Analytically-predicted shear displacements were calculated by using average shear strain values of all the individual model elements that are lined up at the same vertical level multiplied by the element height, and these average shear displacement values are summed over the wall height for obtaining the cumulative shear displacement. The results indicate that the contributions of shear deformations to wall lateral displacements are considerable, and are well estimated by the analytical model for all three specimens at all drift levels. A representative comparison of measured and predicted vertical strain profiles (along the wall cross section) at the bottom of specimen RW-A15-P10-S78 is presented in Fig.5(h), at various drift levels. The model provides reasonably accurate predictions of both compressive and tensile strains, as well as the location of the neutral axis on the wall cross section.

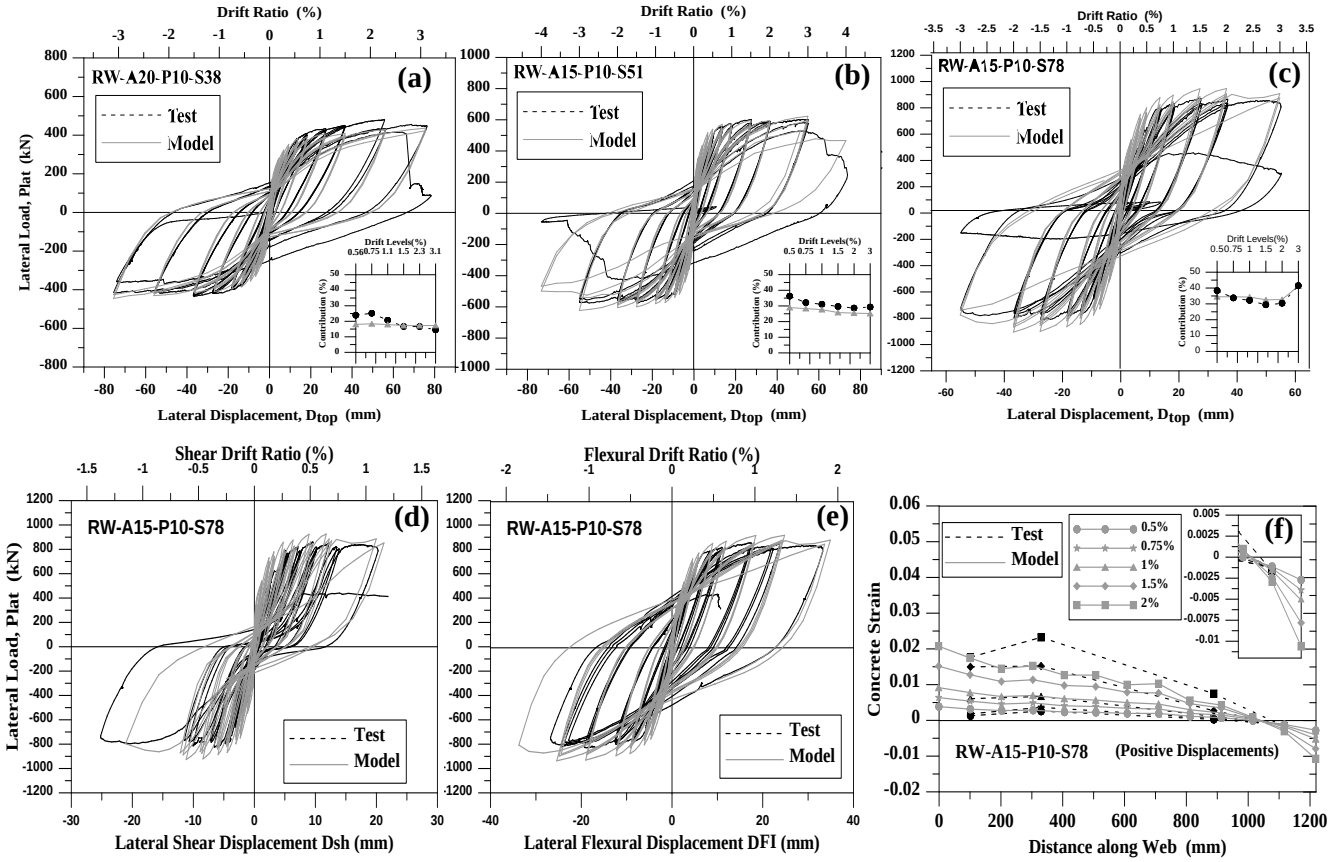

Fig. 5 – Lateral load vs. top displacement responses for a) RW-A20-P10-S38, b) RW-A15-P10-S51, c) RW-A15-P10-S78, d) Lateral load vs. shear displacement for RW-A15-P10-S78, e) Lateral load vs. flexural displacement for RW-A15-P10-S78, f) Vertical strain profile for RW-A15-P10-S78

Validation of the analytical model for walls with flexure-controlled behavior was done using test results of relatively slender (aspect ratio 3.0) wall specimens tested by Thomsen and Wallace [7] with rectangular and T-shapes cross-sections. Comparison of the experimentally-measured and analytically-predicted lateral load vs. top displacement response of the rectangular wall specimen RW2 is presented in Fig.6(a). As can be observed in the figure, the analytical model captures, with reasonable accuracy, the experimentally-observed lateral load-displacement response of the wall specimen. The analysis was conducted by applying the experimentally-applied top displacement history under a constant axial load level of $7\%A_g f'_c$. The analytically-predicted lateral load vs. displacement response reasonably represents the experimentally-observed cyclic response characteristics of the wall, including lateral load capacity, stiffness degradation, hysteretic shape, plastic (residual) displacements, ductility, and pinching behavior. Overall, the model provides an accurate prediction of the global lateral load response of the wall specimen. The model predictions are also compared with the lateral load vs. shear deformation responses measured along the first story of the wall specimen (bottom quarter of wall height) in Fig.6(b). In the analytical model results, significant nonlinearity in the shear behavior was observed along the first story where nonlinear flexural deformations are concentrated, similarly to the experimental behavior, although the maximum shear deformations were slightly underestimated by the model (Fig.6.(b)). It is anticipated that improving the shear aggregate interlock model and dowel action models in the model formulation will help capture the measured shear deformation values with improved accuracy. Fig.6(c) compares the measured and predicted concrete strain profiles along wall web at selected peak drift levels. As revealed in the comparisons, the measured and predicted strain values are close in both the tension and compression regions of the wall cross-section. As obviously depicted in the figure, unlike in fiber models, plane sections do not necessarily remain plane in the finite element modeling approach used herein, which is more consistent with the experimentally-measured strain profiles and provides much better predictions of compressive strains in concrete. Accurate predictions are also obtained for the depth of the neutral axis.

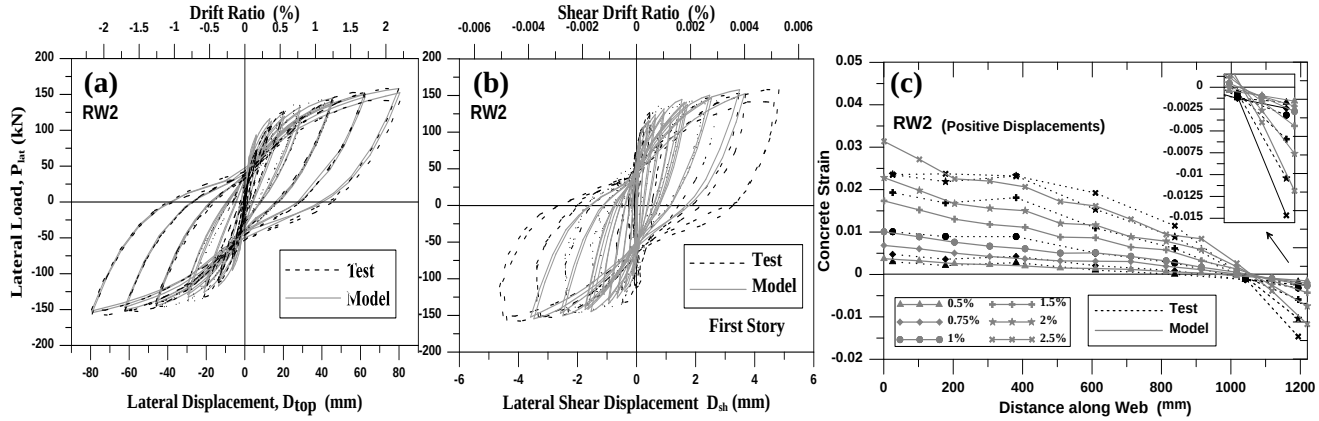

Fig. 6 – a) Lateral load vs. top displacement responses for RW2, b) Lateral load vs. first story shear displacement for RW2, c) Vertical strain profile for RW2

Comparison of the experimentally-measured and analytically-predicted lateral load vs. top displacement response of the slender wall specimen with a T-shaped cross-section (TW2, Fig.7(a)) is presented in Fig.7(b). The significance of this validation is to evaluate the capabilities of the proposed model in predicting the response of three-dimensional walls with non-rectangular cross-sections. As shown in Fig.7(b), the analytical model gives reasonably accurate results for the overall load-displacement behavior of the T-shaped wall specimen. The load vs. shear deformation behavior along the first story (bottom quarter of the height) of the wall was also compared with model predictions in Fig.7(c). Results shown in Fig.7(b) reveal that the overall load vs. displacement response prediction of the model is reasonable, although the lateral loads were slightly under predicted by the model when the flange of the wall is in compression, and slightly overestimated when the flange is in tension. The model was again successful in capturing the nonlinear shear behavior along the first story of the wall (where nonlinear flexural deformations are concentrated); however, shear deformations were notably overestimated in the negative loading direction when wall flange is in tension.

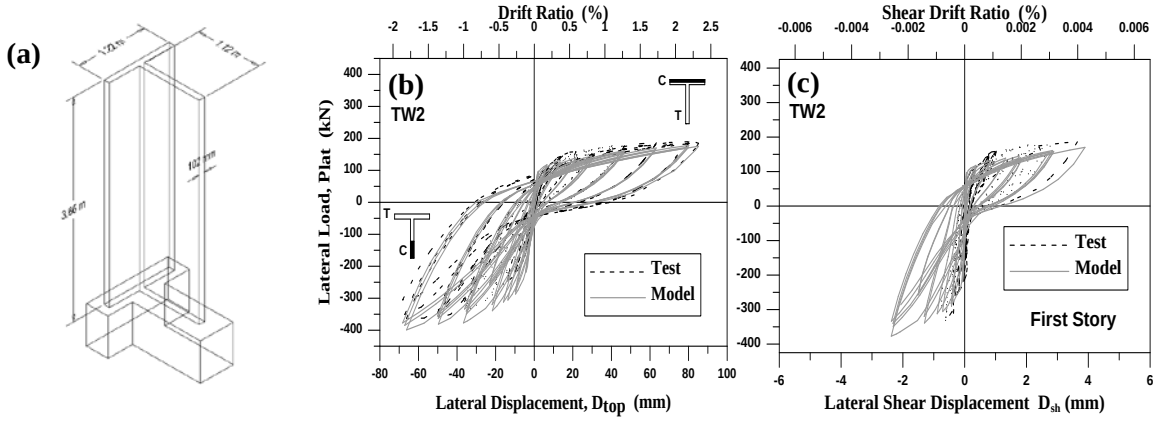

Fig. 7 – a) 3D view of TW2 b) Lateral load vs. top displacement responses for TW2, c) Lateral load vs. first story shear displacement for TW2

Experimentally-obtained responses for squat wall specimens with shear-dominant responses were also compared with predictions of the analytical model. Among the wall specimens investigated, specimen SW-T1-S1-2 had an aspect ratio of 0.5, and there was no axial load applied on this specimen. The measured and predicted lateral load vs. top displacement responses for specimen SW-T1-S1-2 are compared in Fig.8. The failure mode of this specimen was diagonal tension, where crushing of concrete initiated and propagated along diagonal struts. The initial stiffness of the wall specimen is reasonably captured by the analytical model, although the stiffness after cracking was overestimated. The lateral load capacity of the specimen was slightly overestimated in the negative loading direction, whereas it was well-predicted in the positive loading direction.

For this specimen, at 1.2% drift level, concrete started to crush at the center of the wall, initiating strength degradation. The model underestimated the ductility for the wall; however, degradation of the lateral load and pinching behavior were represented fairly well. Specimen SW-T1-N10-S1-11 an identical specimen; however, it was tested under an axial load level of $10\%A_g f'_c$. As depicted in Fig.9, the model captures the lateral load capacity of this specimen (especially in the positive loading direction), overestimates its stiffness, underestimates its ductility, and reasonably represents its lateral load degradation and pinching characteristics. This specimen experienced sudden strength degradation in the positive loading direction due to crushing of concrete, whereas degradation in the analysis results was more gradual, as is typically the case with the model results. For these two specimens, the analytical response was found to be significantly sensitive to the parameters of the constitutive models adopted for aggregate interlock and dowel action, indicating that using more refined constitutive relationships for interlock and dowel may potentially improve the model accuracy.

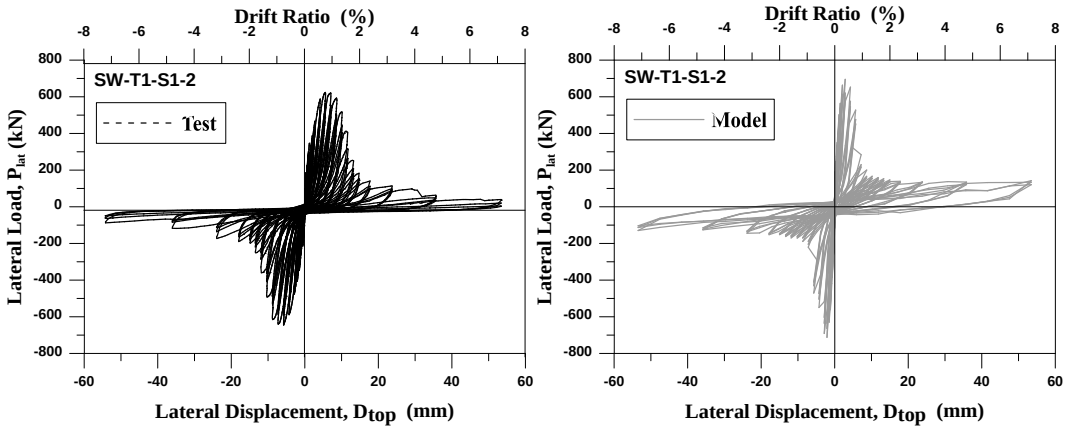

Fig. 8 – Lateral load vs. top displacement responses for SW-T1-S1-2

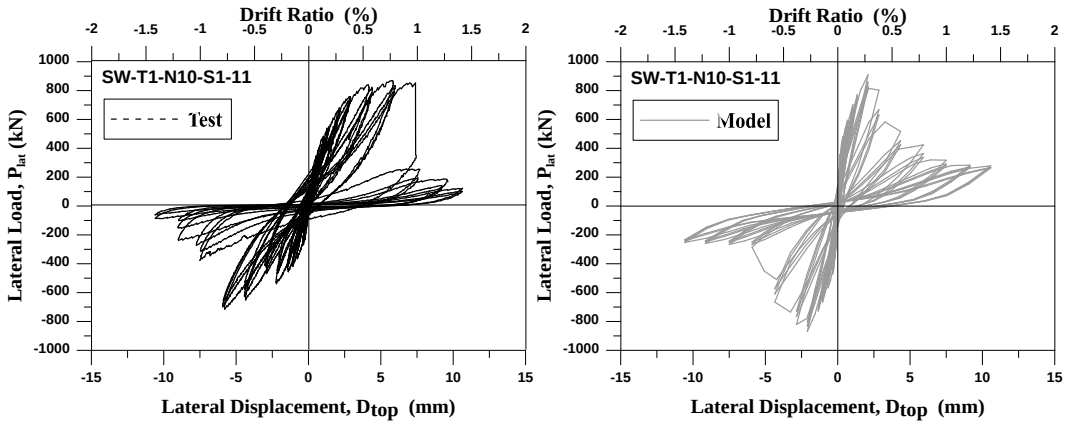

Fig. 9 – Lateral load vs. top displacement responses for SW-T1-N10-S1-11

As shown in Fig.10 for specimen WP-T5-N5-S1, which was subjected to an axial load corresponding to 5% of its axial load capacity, the model exhibited good accuracy in predicting the stiffness, lateral load capacity, and ductility characteristics of the wall, in both positive and negative loading directions. The failure mode of this specimen was formation of diagonal cracks followed by crushing of concrete at the wall center, resulting in pronounced degradation in the lateral load. This degradation in lateral load, although captured by the model, was more gradual in the analytical results. A similar correlation was obtained for specimen WP-T5-N10-S2, subjected to as axial load corresponding to 10% of its axial load capacity. The response was well-predicted by the model in terms of stiffness, lateral load capacity, and ductility (Fig.11). The failure mode of this specimen was also crushing of concrete at the wall center, resulting in sudden degradation in lateral load, which was captured by the model, although the model predicted relatively more gradual degradation. It is a significant

attribute that the overall response prediction of the model for the axially-loaded wall specimens is accurate, because the model is apparently successful in representing the influence the axial load on the shear-controlled response characteristics of walls. Considering that seismic design codes and performance assessment guidelines neglect the influence of axial load in calculation of the shear strength and stiffness of RC walls, mainly due to lack of experimental data, availability of a modeling approach considering interaction between axial load and shear capacity is promising towards improvement of code provisions on wall shear strength.

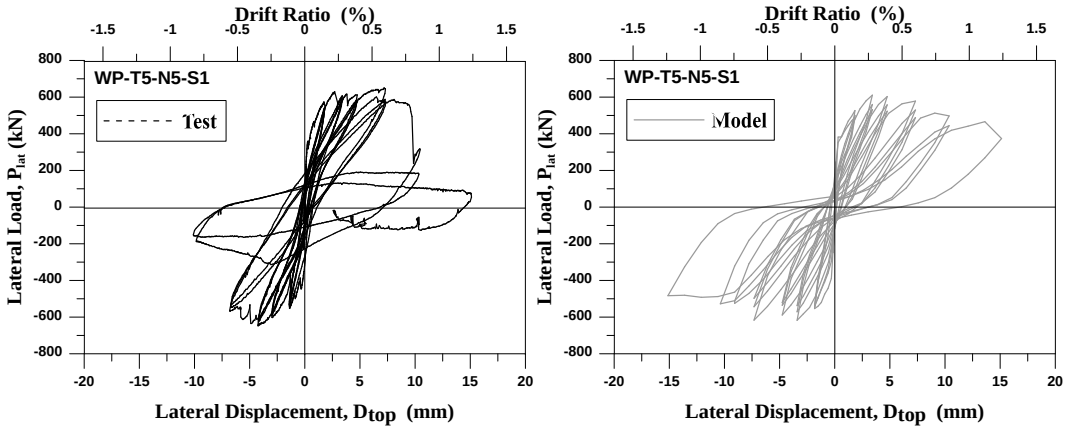

Fig. 10 – Lateral load vs. top displacement responses for WP-T5-N5-S1

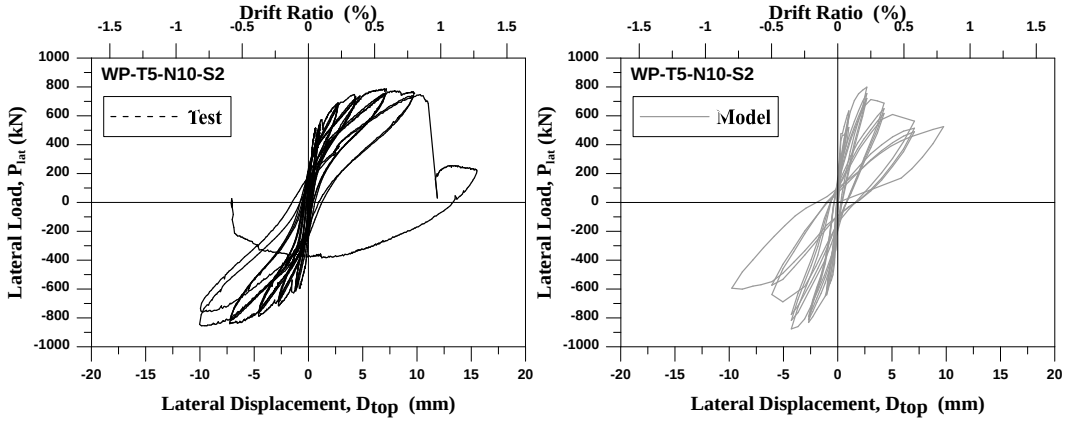

Fig. 11 – Lateral load vs. top displacement responses for WP-T5-N10-S2

4. Conclusion

The finite element modeling approach adopted in this study demonstrated a reasonable level accuracy in predicting the nonlinear hysteretic response of reinforced concrete structural walls with various aspect ratios, cross-sectional geometries and reinforcement characteristics under reversed-cyclic loading conditions. Response comparisons with test results on all wall specimens revealed that the model provides reasonable predictions of the overall lateral load vs. displacement response characteristics of the walls investigated, also capturing the influence of the level of axial load on the observed response.

The model also provides reasonably accurate estimates of the relative contribution of flexural and shear deformations to wall displacements. The model results show nonlinear shear deformations developing along the plastic hinging region of the relatively slender wall specimens, indicating that the model can capture coupling of nonlinear flexural and shear deformations even in slender walls. In medium-rise walls, where shear-flexure interaction behavior is predominant, the model can correctly predict the contribution of flexural and shear deformations on the response throughout the entire loading history. Simulation of shear-flexure interaction

responses in slender and medium-rise walls is one of the significant advantages of the finite element modeling approach adopted in this study, over commonly-used fiber model formulations that consider uncoupled flexural and shear responses. Average longitudinal strain profiles along the base of slender and medium-rise walls are also predicted by the model with reasonable accuracy, in both tension and compression regions of the wall cross-section. Unlike in fiber models, plane sections do not necessarily remain plane in the proposed finite element model formulation, which is more consistent with the experimentally-measured strain profiles and provides better predictions for the compressive strains in concrete, compared to fiber model formulations.

As well, the adopted modeling approach is shown to be capable of simulating the nonlinear hysteretic response of low-rise structural walls under cyclic loading, with an acceptable level of accuracy. It was anticipated that predictions of the analytical model for squat walls will be improved upon implementation of more refined constitutive relationships for shear aggregate interlock and dowel action mechanisms in the model formulation.

5. Acknowledgements

The authors would like to thank Prof. John Wallace and Dr. Thien Tran from UCLA and Prof. Kristijan Kolozvari from California State University Fullerton for sharing test data.

6. References

[1] Tran TA, Wallace JW (2012): Experimental study of nonlinear flexural and shear deformations of reinforced concrete structural walls. *15th World Conference on Earthquake Engineering*, Lisbon, Portugal.

[2] Orakcal K, Wallace JW (2006): Flexural modeling of reinforced concrete walls – model calibration. *ACI Structural Journal*, **103** (2), 196-206.

[3] Massone LM, Orakcal K, Wallace JW (2006): Modeling of squat structural walls controlled by shear. *ACI Structural Journal*, **106** (5), 646-655.

[4] Gullu MF (2013): Finite element modeling of reinforced concrete structural walls. *MS. Thesis*, Boğaziçi University, Istanbul, Turkey.

[5] Ulugtekin D (2010): Analytical modeling of reinforced concrete panel elements under reversed cyclic loadings. *MS. Thesis*, Boğaziçi University, Istanbul, Turkey.

[6] Orakcal K, Ulugtekin D, Massone LM (2012); Constitutive modeling of reinforced concrete panel behavior under cyclic loading. *15th World Conference on Earthquake Engineering*, Lisbon, Portugal.

[7] Thomsen JH, Wallace JW (1995): Displacement-based design of reinforced concrete structural walls: An experimental investigation of walls with rectangular and t-shaped cross-sections. *Report No. CU/CEE-95/06,* Department of Civil Engineering, Clarkson University, Postdam, New York.

[8] Massone LM (2006): Analytical and experimental with shear - flexure interaction in RC walls. *Ph.D. Thesis*, University of California.

[9] Orakcal K, Massone LM, Wallace JW (2009): Shear strength of lightly reinforced wall piers and spandrels. *ACI Structural Journal*, **106** (4), 455-465.

[10] Terzioglu T (2011): Experimental evaluation of the lateral load behavior of squat structural walls. *MS. Thesis*, Boğaziçi University, Istanbul, Turkey.

[11] Chang GA, Mander JB (1994): Seismic energy based fatigue damage analysis of bridge columns: Part I-Evaluation of seismic capacity, *NCEER Report No. 94-0006*, National Center for Earthquake Engineering Research, Buffalo, USA.

[12] Menegotto M, Pinto E (1973): Method of analysis for cyclically loaded reinforced concrete plane frames including changes in geometry and non-elastic behavior of elements under combined normal force and bending. *IABSE Symposium on Resistance and Ultimate Deformability of Structures Acted on by Well-Defined Repeated Loads*, Lisbon, Portugal.

[13] Thermou GE, Papanikolaou VK, Kappos AJ, (2011): Analytical model for predicting the response of old-type columns rehabilitated with concrete jacketing under reversed cyclic loading", COMPYDN, Greece.

[14] Karabulut S (2016): Nonlinear response modeling of low-rise structural walls. *MS. Thesis*, Boğaziçi University, Istanbul, Turkey.

[15] He XG, Kwan AKH (2001): Modeling dowel action of reinforcement bars for finite element analysis of structures. *Computers and Structures*, **79** (6), 595-604.

[16] Horoz B, Gullu MF, Orakcal K (2015): Modeling of coupled nonlinear shear and flexural responses in medium-rise RC walls. *Third Conference on Smart Monitoring, Assessment and Rehabilitationof Civil Structures*, Antalya, Turkey.

[17] Kolozvari K, Tran T, Wallace JW, Orakcal K (2014): Modeling of cyclic shear-flexure interaction in reinforced concrete structural walls. I: Theory", *ASCE Journal of Structural Engineering*, **141** (5), 541-550.